Pergamon

Cement and Concrete Research, Vol. 28, No. 12, pp. 1737–1751, 1998

0008-8846/98 $–see front matter

PII S0008-8846(98)00156-2

ASSIGNMENT OF FEATURES IN IMPEDANCE SPECTRA OF THE CEMENT-PASTE/STEEL SYSTEM

S.J. Ford, J.D. Shane, and T.O. Mason[1]
Center for Advanced Cement-Based Materials, Northwestern University, Department of Materials Science and Engineering, Evanston, IL 60208-3108, USA

(Received March 9, 1998; in final form September 1, 1998)

ABSTRACT

This paper presents a systematic study of the features seen in typical Nyquist plots (-imaginary vs. real impedance) for cement-paste/steel systems and discusses the assignment of each feature to its appropriate origin, e.g., bulk, contact, interface, product layer, etc. Assignments are made based upon as many considerations as possible—dc measurements, sample geometry, capacitance, local chemical modifications, alternative electroding schemes, etc. In addition to three distinct arcs from lowest (mHz) frequency to highest (MHz) frequency (due to product layer, interfacial reaction, and bulk, respectively), a fourth arc is sometimes observed between the bulk and interface arcs. When this occurs in paste-only systems, this arc is attributable to imperfect electrodes due to drying/shrinkage. In composite systems, e.g., cement with conductive chopped fibers added, this arc is clearly a "bulk" feature and an important indicator of microstructural inhomogeniety.

Introduction

Figure 1 illustrates the basics of impedance spectroscopy (IS) for the characterization of microstructure in materials science. A PC-controlled frequency response analyzer (FRA) is employed to interrogate a system (material under study plus electrodes) with small amplitude AC signals of varying frequencies and to collect gain and phase angle information. These data are converted to Nyquist format (-imaginary vs. real impedance), from which various equivalent circuit elements are derived. Physical intuition allows association of specific features with underlying processes/features in the microstructure of the material under study, e.g., the grains and grain boundaries in an electroceramic specimen. An excellent review of experimental and theoretical considerations is given in the monograph of Macdonald (1).

Meaningful microstructural interpretation and equivalent circuit modeling require the collection of reliable impedance data. In prior works we identified a number of experimental limitations—stray apparatus imittances (2), electrode contact effects (3), and reference electrode problems [for multipoint IS, see refs. (4–7)]—which must be considered and

[1]To whom correspondence should be addressed.

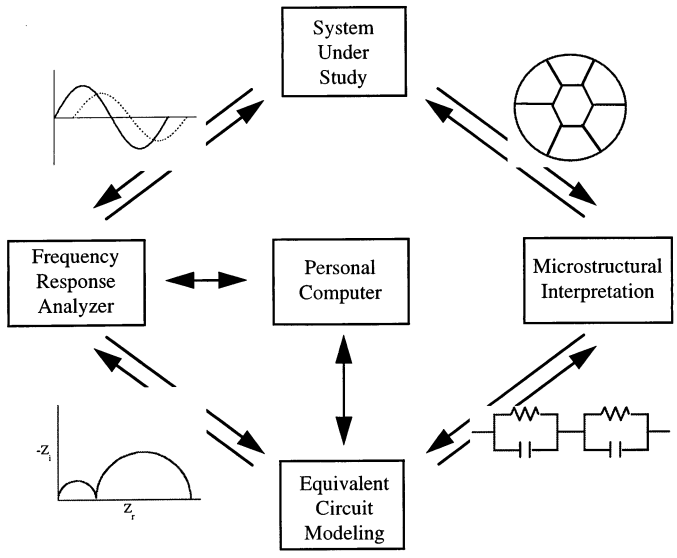

FIG. 1.
Schematic representation of the basic elements of impedance spectroscopy in materials science.

controlled. Assuming that reliable data are obtained, an important but often overlooked step in the IS "loop" of Figure 1 is the assignment of individual Nyquist features to the responsible regions of the system under study, e.g., bulk, contacts, electrode reactions, product layers, etc. The present work addresses the proper assignment of IS Nyquist plot features in cement-paste/steel systems.

From the first application of IS to cement-based materials (8,9), multiple features were observed. Figure 2 shows a Nyquist plot from Scuderi et al. (9) showing four characteristic features. Because these four (or at least three) features are commonly observed in impedance spectra, the present work will adopt the designations A, B, C, and D, throughout. It should be pointed out that the lowest frequency feature (A) is an arc whose maximum imaginary component occurs in the mHz range. Spectra taken at higher frequencies will see fewer features, e.g., D and C only, or D plus C with a hint of component B, e.g., McCarter et al. (8). Feature B can be a distinct arc, as we will show, but can often be overwhelmed by the size of arc A. (In Fig. 2 the fitting line for arc A is shown to emphasize the existence of response B.) In the original work by Scuderi et al. (9), an additional letter, "E," was employed to reflect the nonzero real impedance offset of feature D. Because IS data are unreliable above 10 MHz, we will restrict our discussion to the four features in Figure 2. (Note that because feature D is clearly attributable to the cement paste bulk [see below], any higher frequency feature, regardless of microstructural origin, will likewise originate from the bulk.)

There are several bases for assigning individual Nyquist features to the underlying regions in the system under study.

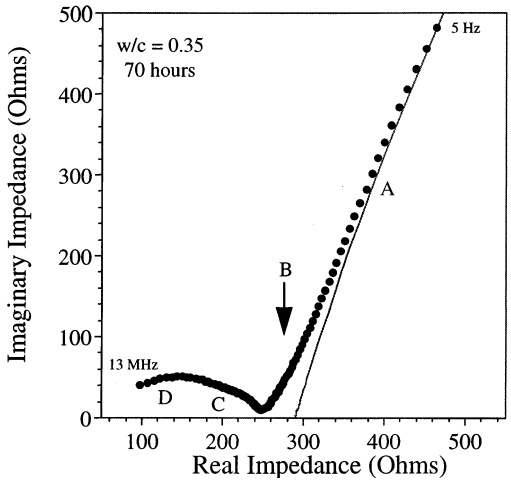

FIG. 2.
An early Nyquist plot from Scuderi et al. (9). An extension of the arc used to fit feature A is shown to emphasize the existence of feature B.

Removal of elements

Electrode-related features can be identified by removing the cement paste and replacing it with simulated pore solution (SPS). Similarly, bulk-related features can be identified by "removing" the electrodes (see "Alternative Electroding Strategies" following.

Geometry

Bulk-related features should scale with the aspect ratio of the specimen under study, i.e., bulk resistance should scale linearly with the length-to-cross-sectional area (l/A) and capacitance should scale with the inverse of l/A. In contrast, electrode-related features (e.g., product layers, reaction processes) should scale only with electrode area and not with sample length.

Capacitance

Irvine et al. (10) provide a useful table for making IS feature assignments based upon capacitances. A modified version of this table is shown in Table 1. Table 1 assumes an l/A ratio of 1 cm^{-1} and an A of 1 cm^2 and takes into account the higher dielectric constant of a water-based material like cement paste ($\epsilon_r = 80$). We have also considered product layers ($\epsilon_r = 10$) from 10 nm to 10 μm in thickness. What is most important about Table 1 is the discrimination between bulk-related (low capacitance) and electrode-related (high capacitance) features.

TABLE 1
Capacitance values and their possible interpretations.

Capacitance (F)	Phenomena responsible	Bulk vs. electrode origin	Frequency regime
10^{-11}	Bulk	Bulk	MHz
10^{-10}–10^{-8}	Internal space charge layers*	Bulk	kHz–MHz
10^{-7}–10^{-4}	Product layers	Electrode	mHz–Hz
10^{-4}	Electrochemical reactions	Electrode	mHz

* Grain boundaries in electroceramics.

Local chemical/structural modifications

Preferential modifications can be made to the product layer (by changing the steel chemistry), to the electrochemical reactions at the cement-paste/steel interface (by dip-coating the electrode with silica fume), and to the bulk (by chemical/mineral admixtures). These are described more fully in the following.

Alternative electroding schemes

Typically, the intersection between features B and C in Figure 2 is taken to be the total bulk resistance. This should always be verified by four-point dc resistance measurements, which is the best means of establishing that features A and B are electrode related rather than bulk related. We will show, however, that imperfect electrodes (due to shrinkage and/or drying) can be responsible for feature C. In such cases, the dc four-point resistance will agree with the low-frequency intercept of arc D instead of the C/B intercept. As additional confirmation, the steel electrodes can be removed and replaced with low-resistance electrodes (e.g., silver paint) for two-point IS measurements, thereby removing feature C.

It should be stressed, however, that a truly bulk feature C can be obtained in certain instances, e.g., steel fiber-reinforced cement paste with steel electrodes. In such cases the four-point dc resistance will agree with the sum of the D and C resistances, i.e., the C/B intercept in Figure 2.

Experimental

Specimens

Pastes were prepared using type I ordinary portland cement (OPC) and distilled water and mixed in a Hobart planetary mixer for 15 minutes. Samples were cast in rectangular Plexiglas molds, 2.5 × 2.5 × 10 cm. Except where otherwise noted, low carbon (C-1018) steel coupons were employed as electrodes. These were polished to 600 grit, cleaned with acetone, rinsed with distilled water, and cast in place at the ends of each specimen. The embedded area

was ~5 cm^2. The composition of the C-1018 steel was, in weight percent (wt%), 0.15–0.2 C, 0.6–0.9 Mn, and <0.04 and 0.05 P and S, respectively.

Impedance measurements

IS measurements were made using either a Solartron 1260 or a Hewlett-Packard (HP) 4192A FRA. In most cases an excitation signal of 25 mV was employed, at zero bias. Frequency was swept from 20 MHz (or 13 MHz for the HP 4192A) to 2 mHz (5 Hz for the HP 4192A) with data taken at 10 (Solartron) or 20 (HP 4192A) points per decade. Specimens were stored in 100% relative humidity (RH) chambers during hydration. Also, during IS data collection, samples were maintained in a humidity chamber attached to the front of the FRA. An RH sensor was employed to confirm that RH remained near 96% throughout all experiments. The software program, "Equivalent Circuit" (11), was employed to derive resistance and, in some instances, capacitance values from the experimental Nyquist plots.

Alternative electroding and four-point dc resistance measurements

In certain cases, the steel electrodes were broken free from the extremes of the rectangular specimens. These ends were then ground plane/parallel and silver paint (Fullam, Inc., Latham, NY) was applied to them for subsequent two-point IS measurements. For four-point dc resistance measurements, two bands of silver paint ~2 mm wide were applied around the bar at the ~1/3 and 2/3 positions between the Ag-coated ends. The outer electrodes served as current contacts and the inner bands served as voltage contacts for conventional four-point dc resistance measurements. To minimize polarization and avoid Joule heating of sample and/or contacts, low currents were employed (≤5 mA) for brief periods of time, and ohmic behavior was confirmed.

Synthetic pore solution studies

Simulated pore solution (SPS) was made up to simulate the pore solution of an OPC paste with water-to-cement (w/c) ratio 0.5 at 100 h of hydration (12). The constituents were 0.1M NaOH and 0.175M KOH, corresponding to a pH of 13.5. Minor constituents such as S, Si, Ca, and Al were ignored because of their low concentrations (μM) in OPC paste pore solutions at most early hydration times.

System modifications

For the modified product layer experiments, AISI 302 stainless steel (0.15 wt% C, 2 Mn, 1 Si, 17–19 Cr, and 8–10 Ni) and "weathering steel" (0.15 wt% C, 1.16 Cu, 0.44 Ni, 0.54 Mn, and 0.8 Si) coupons were employed and cast similarly to the C-1018 coupons described previously. The weathering steel electrodes were first polished to 600 grit and cleaned with acetone, whereas the stainless steel electrodes were cleaned without polishing. It is well known that silica fume greatly increases the bulk resistance of cement pastes (13). Intentional modification of the electrochemical reaction kinetics at the cement-paste/steel interface was accomplished by dip-coating C-1018 steel electrodes with silica-fume slurry (Force 10,000;

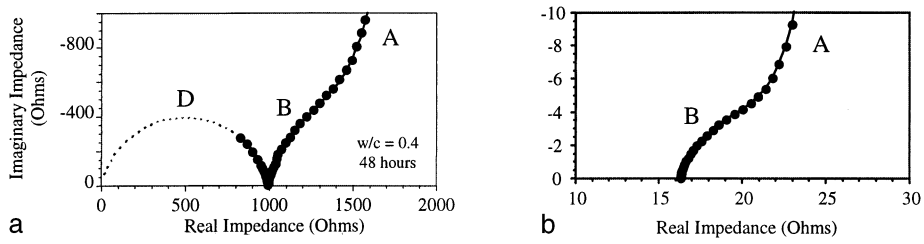

FIG. 3.
Nyquist plots of low carbon steel electrodes in (*a*) ordinary Portland cement and (*b*) synthetic pore solution.

W.R. Grace, Cambridge, MA) followed by drying and casting in OPC paste as described previously. There are numerous literature examples of chemical and/or mineral admixture modifications of the bulk IS response of OPC paste [see refs. (14,15) and the citations therein). In the present work, short steel fibers ~2 mm long and ~30 μm in diameter (Novocon, Inc., Greenville, SC) were dry-mixed with OPC powder for 1 min in a Hobart blender, followed by addition of distilled water and further mixing for 15 min. Electrode/sample casting was as described previously.

Results and Discussion

The low-frequency (electrode-related) features

Figures 3a and 3b compare typical Nyquist plots for C-1018 steel electrodes in OPC paste (w/c = 0.4, 48 h) and in SPS, respectively. It is immediately obvious that neither feature A or B is significantly affected by the presence of the cement paste. The absence of an arc at high frequencies (D) for the SPS case is to be expected due to the high conductivity and relatively low capacitance of SPS, i.e., any electrolyte "arc" would be in the GHz range and beyond the frequency limits of conventional IS measurements. Although not shown here, the fitting parameters for arcs A and B are quite similar in the OPC vs. SPS situations.

The results of aspect ratio studies for the OPC paste/steel system are shown in Figures 4a and 4b. As pointed out in the Introduction, only bulk-related features should have resistances and capacitances that scale with sample geometry. As shown in Figures 4a and 4b, neither feature A nor B exhibits the expected linear relationship with sample length (for resistance) or inverse length (for capacitance). In fact, the parameters for features A and B tend in the opposite direction. (The linear relationships obtained for feature D are discussed further in the following.)

The capacitance values (obtained by equivalent circuit modeling of Nyquist plots for arc A and by imaginary vs. real capacitance plots for feature B, see following) are quite different for the low-frequency features (0.1 to 1-mF range) as compared to feature D (10- to 100-pF range). Such large values are characteristic of product layers and electrochemical reactions, i.e., electrode-related phenomena (see Table 1).

In addition, the results of four-point dc resistance measurements are definitive. The dc

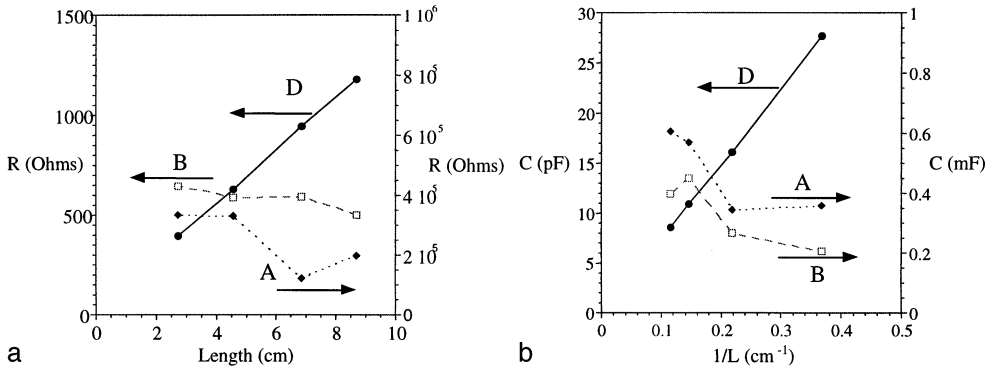

FIG. 4.

Changes in IS feature (*a*) resistance and (*b*) capacitance due to changes in sample geometry. See text for how individual capacitances were obtained. L, length.

resistivity, when appropriately corrected for the small differences in geometry between four-point (dc) and two-point (IS) specimens, always falls at or to the left of the high-frequency B intercept with the real axis in Figure 3a. In other words, A and B features are unquestionably associated with the electrode interface and are not bulk in nature.

Feature A: A product layer

The consensus in the literature is that feature A is associated with an extremely resistive product layer formed when a passive oxide film grows on the steel electrode due to the high pH of OPC pore solution (16–19). The relaxation frequency at which feature A appears depends on many factors such as the presence of admixtures, chlorides, the degree of hydration, the type of steel used, etc., but is typically in the mHz range (see Table 1). The value of capacitance obtained (~0.5 mF) is consistent with an iron oxide film on the order of 10 nm thick, assuming typical dielectric constants for iron oxides (~10). This is entirely consistent with prior reports (18–20). It should be stressed that arc A is typically an almost perfect semicircle, i.e., depression below the real axis tends to be minimal. Using the standard "constant phase element" analysis (1):

$$Z(\mathrm{CPE}) = B(j\omega)^{-n}$$

the values of n obtained by CPE fitting of arc A are always ≥ 0.9 when electrodes are appropriately polished. (A value of $n = 1$ corresponds to a perfect capacitor.) Using the film thickness calculated from the capacitance (~10 nm), an oxide resistivity of 10^{11} TO 10^{12} Ω-cm was obtained, which is typical of passive oxide films (21).

Steel chemistry plays the dominant role in determining the electrical properties of the product layer. In Figure 5 is plotted the size (resistance) of arc A vs. time for three different electrode compositions. The resistance increases by an order of magnitude from plain carbon steel to stainless steel. On the other hand, it decreases by nearly an order of magnitude when "weathering" steel is substituted for plain carbon steel. In contrast, changes in the size

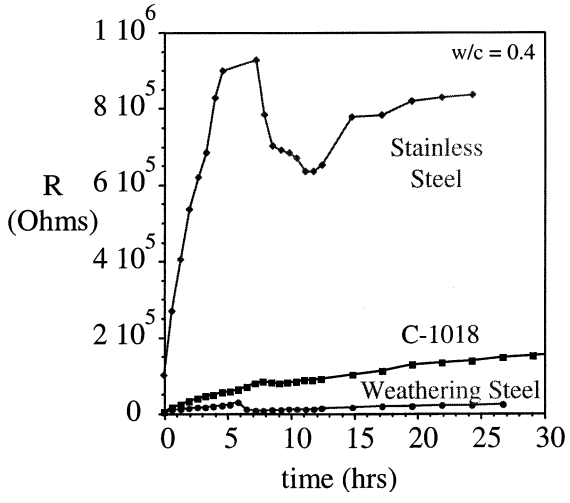

FIG. 5.
The size (resistance) of arc A vs. hydration time for three different steels in ordinary Portland cement paste.

(resistance) of arc A with changes in cement paste formulation (w/c ratio, silica fume additions) are relatively minor. Although the pore solution is the oxidizing agent, the cations for the oxide film are derived from the steel.

The one additive to cement paste pore solution or SPS that can significantly impact the product layer is chloride ions. Elsewhere we describe how additions of sodium chloride to SPS result in the rapid decrease of the diameter of arc A (by three to four orders of magnitude), obviously associated with the pitting of the oxide film and onset of active steel corrosion (22).

Feature B: Electrochemical reaction

There have been several prior reports of feature B in IS measurements on corroding systems (23–27). Because features B and A have a high degree of overlap, it is difficult to accurately determine the frequency range in which it appears. However, based on the values of resistance and capacitance, the relaxation frequency can be estimated to be on the order of 10 to 100 Hz. Two suggested possibilities for this arc are corrosion products formed in the pores of the cement paste or the formation of a $Ca(OH)_2$ layer at the cement-paste/steel interface (26–29). The fact that feature B is also observed in the absence of cement paste (see Fig. 3b) indicates that neither mechanism is responsible in the SPS case. It should be noted that the SPS employed in the present study had no Ca ions as a source of $Ca(OH)_2$. No corrosion products (other than the oxide film discussed previously) are anticipated in the passivation regime.

Due to the extensive overlap of arcs A and B, equivalent circuit modeling and extraction of reliable values for the electrical properties of arc B, especially the capacitance, can be difficult. We have had success plotting the imaginary vs. real components of capacitance as

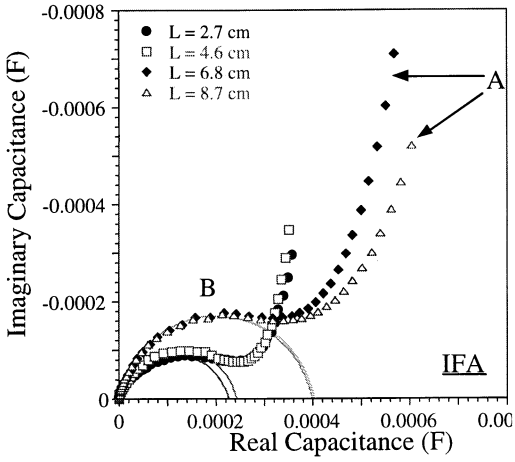

FIG. 6.

Capacitance for four OPC/steel specimens of varying length, plotted in the complex plane. Frequency increases from right to left. The solid lines are nonlinear least-squares fitting results for arc B.

in Figure 6, from which the diameter of the high-frequency (leftmost) arc gives the capacitance of arc B. These capacitances (see Fig. 4b) are typically in the 0.1- to 1-mF range (see Fig. 4b), corresponding to $\sim$20 μF/cm^2, which is consistent with typical values for ionic double layers at electrodes in electrochemical reactions (22,23).

We have interpreted the B arc in SPS as a charge-transfer resistance/double-layer capacitance at the electrolyte (SPS)/steel interface (22). What is unusual about the B feature is its hybrid character in cement-paste/steel systems, i.e., it possesses some attributes of both bulk-like and electrode-like behavior. This can be seen in Figures 4a and 4b, where the resistance is similar to bulk values but the capacitance is clearly typical of an electrode-related response. Another bulk-like characteristic is the time dependence of the B arc resistance. In Figure 7 this parallels the bulk resistance (from the D feature, see following). The inset diagram shows the virtually constant ratio of resistances for the B arc and the bulk (D) arc. Our interpretation is that the B response is associated with the electrochemical reaction (charge transfer-resistance/double layer-capacitance) at the pore-solution/steel interface, but that the area where this reaction can take place is constantly decreasing as the pore fraction in the interfacial transition zone (ITZ) decreases due to hydration. In other words, ITZ porosity, which mimics bulk porosity in its time (and degree of hydration) dependence, modifies the active area over which electrochemical reaction can take place. Given that silica fume is known to significantly increase the bulk resistance of cement pastes, electrode dipping experiments were performed. C-1018 steel electrodes were prepared as described previously, dipped in silica fume slurry, dried, and subsequently cast in cement paste bars for IS measurements. Figure 8a shows how feature B is modified by the silica fume dipping in comparison with an undipped specimen in Figure 8b. The dipped response shows the distinctive 45° angle characteristic of a "Warburg" response. The corresponding *n* value in Eq. 1 is 0.5. This behavior is indicative of diffusion control adjacent to the electrode/

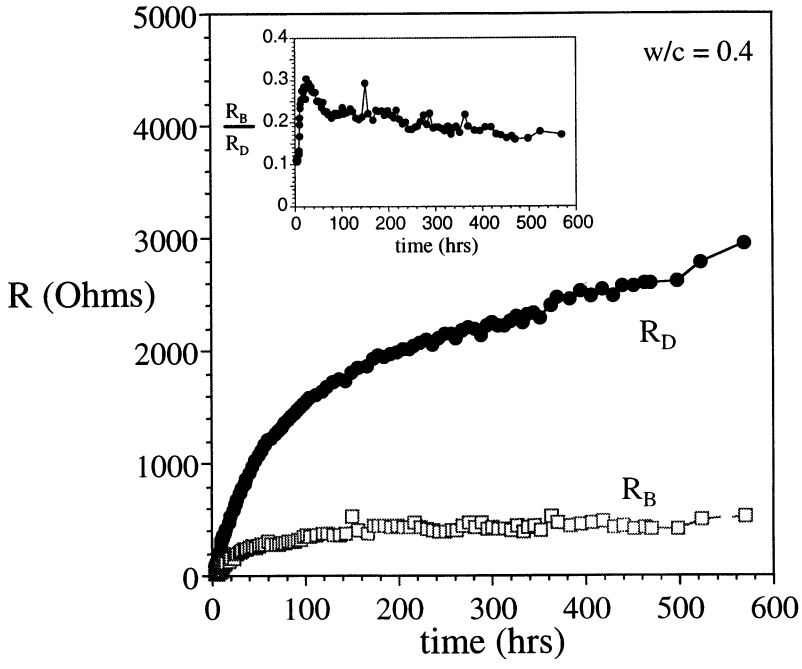

FIG. 7.
Time evolution of arc D (bulk) and arc B in the OPC/steel system. The inset diagram shows that the ratio of these resistances remains virtually constant during hydration.

cement interface (1). In other words, the silica fume added to the interface region has significantly modified the ITZ, and this diffusional resistance now dominates over the charge-transfer resistance. [Note that the bulk (D) arc is relatively unaffected by the dipping, and although not shown here, the product layer (A) arc is also relatively unaffected by dipping.] We have previously documented similar Warburg-like behavior with steel electrodes in bulk cement paste containing silica fume (30).

Little attention has been paid in the literature to arc/feature B in impedance spectra of the cement-paste/steel system. Although arc B is associated with electrochemical reactions at the cement-paste/steel interface, it can be modified by the ITZ porosity immediately adjacent to the steel surface. The ability to render the ITZ less porous and therefore less diffusible, e.g., by the addition of small pozzolanic particles to the ITZ and/or bulk, is a potentially important means of corrosion control.

The high-frequency (bulk-related) features

Features C and D in Figure 2 only occur when cement paste is present (see Fig. 3). It is therefore logical to assume that these are both "bulk" features. For example, it is routinely assumed that the high-frequency (leftmost) real impedance intercept of feature B is the true bulk resistance of the cement specimen. In most instances this is a correct assumption (see

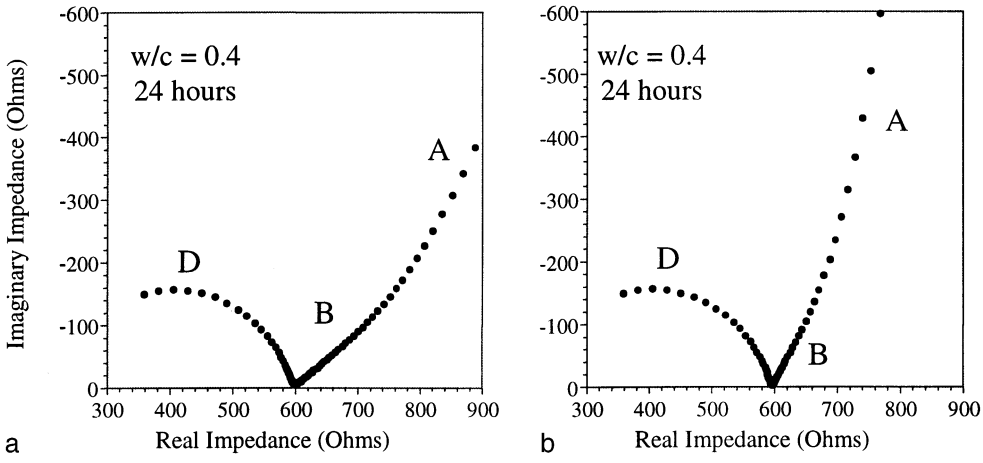

FIG. 8.
Nyquist plots of steel electrodes in ordinary portland cement paste with (*a*) and without (*b*) silica fume precoating.

Fiber Composites following). However, we have found that imperfect electrodes, due to local drying and/or cracking, can yield Nyquist plots with an erroneous feature C, and for which the C/B real axis intercept does not agree with four-point dc resistance measurements.

Paste-only features

Without dispersed particles (e.g., fibers) and with good electrode contacts, only arc D is observed (see Figs. 3a, 8a, and 8b). In this case, the D arc begins in the kHz range with a relaxation frequency (frequency at the top of the arc) of about 10 MHz. In every case we obtain excellent agreement between four-point dc resistance and the D/B intercept in the Nyquist plots. Furthermore, the resistance (obtained from equivalent circuit fitting) and the capacitance (taken at 10 MHz from the raw data) vary linearly with specimen geometry (see Fig. 4).

In paste-only systems, feature C can arise when electrode drying and/or cracking takes place. This is demonstrated in Figure 9. In both cases, the C arc appears in the kHz range. These are two different spectra for an OPC paste with 20% silica fume (w/s ratio = 0.4) and stainless steel electrodes, aged in 100% RH for approximately 5 months. Notice the presence of feature C for the "aged" samples. Note also the disparity between the C/B intercept and the four-point dc resistance value. Upon rewetting of the electrodes (Fig. 9a) or removal of the steel electrodes and replacement with silver paint electrodes (Fig. 9b), feature C disappears and now the low-frequency (rightmost) D intercept agrees well with the 4-point dc resistance value. It is noteworthy that the overall response of the "aged" sample in Figure 9b closely resembles the Scuderi et al. (9) plot in Figure 2.

We interpret feature C in the "aged" sample to be due to an imperfect electrode contact. Elsewhere we attribute imperfect electrode behavior to "spreading resistance" at a few points where a planar electrode is in contact with the specimen surface (3). The air "gap" between

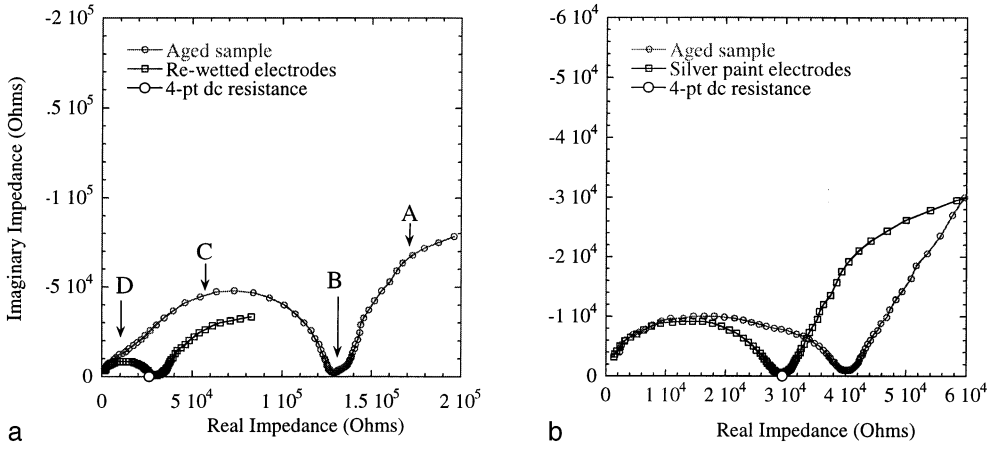

FIG. 9.

Impedance spectra of an OPC/silica fume specimen (age approximately 180 days) with steel electrodes showing an imperfect electrode response before and after rewetting (*a*) or reelectroding with silver paint (*b*). In each panel, the open circle represents the true four-point dc resistance of the specimen. Note that Figure 9b closely resembles Figure 2.

the electrode and the uncontacted specimen surface acts as a parallel plate capacitor. For example, the "aged sample" arc C in Figure 9 has a capacitance of ~0.1 nF, which would correspond to a physical gap of ~50 μm. Upon rewetting (recontacting) or replacement with a more intimate electrode (silver paint), this spreading-resistance/gap-capacitance feature disappears.

There are two possible explanations for the imperfect electrode feature C in cement-paste/steel specimens. First, preferential drying of the ITZ removes the aqueous phase, which is necessary for good electrochemical contact to the steel. We suspect this to be responsible for the appearance of feature C in the earliest Nyquist plots (8,9), e.g., Figure 2. These were performed without proper attention to maintaining saturation (100% RH) throughout the hydration process. For example, it is relatively easy to reproduce the feature C artifact in air-cured OPC/steel specimens. Second, shrinkage cracking also can separate the cement from the steel electrodes. We typically see cracking at the electrodes in pastes with silica fume, even when 100% RH curing is employed. This is undoubtedly due to the enhanced chemical shrinkage of silica fume pastes (31).

Fiber composites

In certain instances a bulk-related feature C can be observed in composite systems. Figure 10 displays the Nyquist plot for an OPC paste with 1% by volume steel fibers (~30 μm diameter × 2 mm long) showing features D and C. Note that in this case the four-point dc resistance agrees with the sum of features D and C rather than just with feature D alone. There were no substantive changes in the high-frequency features (C, D) with alternative electroding schemes (e.g., silver paint). Furthermore, the resistance of each feature (deter-

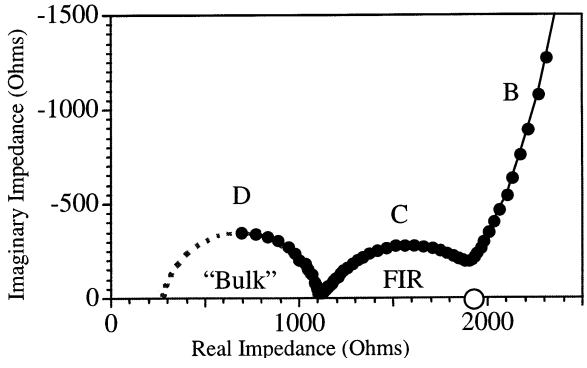

FIG. 10.

Nyquist plot for a neat OPC paste (w/c = 0.4) containing approximately 1% by volume steel fibers. The open circle represents the four-pt dc resistance of the sample.

mined by equivalent circuit fitting) scaled linearly with specimen geometry. Both features C and D are attributable to the bulk of the composite. It should be stressed that neither feature corresponds directly to the bulk D arc in paste-free specimens. Both are part of the bulk IS response. Interpretation of each feature insofar as microstructure is concerned is beyond the scope of this paper. Nevertheless, the appearance of two separate features (C,D) in fiber-reinforced composites indicates that IS is sensitive to microstructural heterogeneities. Chen and Chung (32) have suggested the use of electrical properties to detect microstructural changes during loading of fiber-reinforced systems, i.e., "smart" concretes.

Conclusions

Three, or possibly four, individual arcs/features are typically observed in the Nyquist plots of the cement-paste/steel system (see Figs. 9 and 10). By careful manipulation of specimen geometry, comparison of four-point dc resistance and IS response, "removal" of an element (electrode or cement), intentional modification of local chemistry/microstructure, and alternative electrode schemes, it is possible to correctly assign individual features to the responsible zone/process of the cement-paste/steel system—bulk, imperfect electrode contacts, electrochemical reaction, product layer, etc.

The lowest-frequency feature (A in all the figures) is a large, nearly semicircular arc with a maximum imaginary impedance in the mHz range. This arc is attributable to the passive iron oxide film that forms under the high pH characteristic of saturated cement pastes. It is relatively insensitive to the aqueous phase chemistry, the noteworthy exception being the presence of chloride ions that pit the film, and is largely determined by the composition of the underlying steel. The values of resistivity and dielectric constant obtained from IS fitting are consistent with a continuous ferric oxide film ~10 nm thick.

The next feature (B), as frequency increases, is sometimes difficult to deconvolute from the overwhelming oxide film arc (A). It is also present when the steel is placed in Ca-free synthetic pore solution. We attribute this feature to the electrochemical reaction at the electrode (film) surface and the associated charge-transfer resistance and double-layer ca-

pacitance. In the presence of cement paste, however, these parameters are modified such that $<100\%$ of the electrode surface is exposed to pore solution. Instead, as pore fluid is consumed and hydration product fills pores in the ITZ, the "active" electrode area progressively declines; therefore, the resistance of this feature steadily increases in tandem with the bulk (arc D) resistance. The interesting aspect of this feature is that it may provide a tool for studying the change in microstructure of the ITZ during the course of hydration.

Without second phase additions (e.g., fibers) and in the absence of imperfect electrode contacts, the real axis Nyquist plot intersection of arcs B and D is the true dc resistance of the cement sample (see Figs. 3a, 8, and 9). Arc D is clearly a "bulk" feature whose electrical properties scale linearly with the aspect ratio of the sample. This feature occurs at high frequencies, with the maximum imaginary impedance typically occurring in the 1- to 10-MHz range. Because this is the current limit of reliable IS measurements, the possibility of additional features (e.g., an offset resistance, additional arcs, etc.) cannot be resolved by IS.

We have identified two situations in which an additional feature/arc (C) occurs between the high-frequency arc (D) and the two low-frequency features (A and B). The first occurs when imperfect electrode contacts result from drying of ITZ pores and/or cracking due to cement shrinkage, which pulls the cement away from the steel surface. In such cases, the low-frequency intercept of this feature does not agree with the true dc resistance of the sample. Instead, the D feature is the true bulk response and the C feature derives from "spreading resistance" point contacts and the air–gap capacitance between the cement and the steel electrode. Feature C disappears upon rewetting of the electrode with pore solution or replacement of the steel electrodes with silver paint electrodes.

It should be stressed that it is important to carry out four-point dc resistance measurements in parallel with IS measurements to appropriately detect and assign the high-frequency features. In some cases the imperfect electrode contact feature can be quite large (e.g., with extensive drying/cracking at the electrodes), whereas in other instances it can be quite small (see Fig. 9) and even merge with arc D into a single depressed arc. Although feature C can be eliminated by reestablishing electrode contact (e.g., by rewetting or the use of silver paint), the dc resistance is the surest method to test for the presence of imperfect electrode contacts.

The second situation where an additional feature C has been observed is for cement pastes reinforced with conductive fibers (see Fig. 10). In this case the four-point dc resistance agrees with the sum of resistances D and C, i.e., the low-frequency intercept of feature C with the real axis, which also agrees with the high-frequency intercept of features B and A. In these materials, neither feature D nor C represents the entire "bulk" response. Both are determined by the heterogeneous composite microstructure. It appears that IS is particularly sensitive to the microstructural heterogeneities in such materials and additional IS work on composites is therefore warranted.

Acknowledgment

This work was supported by the NSF Science and Technology Center for Advanced Cement-Based Materials under grant no. CHE-91-20002.

References

1. J.R. Macdonald, Impedance Spectroscopy: Emphasizing Solid Materials and Systems, John Wiley & Sons, New York, 1987.

2. D.D. Edwards, J.-H. Hwang, S.J. Ford and T.O. Mason, Solid State Ionics 99, 85 (1997).
3. J.-H. Hwang, K.S. Kirkpatrick, T.O. Mason and E.J. Garboczi, Solid State Ionics 98, 93 (1997).
4. G. Hsieh, S.J. Ford, T.O. Mason and L.R. Pederson, Solid State Ionics 91, 191 (1996).
5. G. Hsieh, T.O. Mason and L.R. Pederson, Solid State Ionics 91, 203 (1996).
6. G. Hsieh, T.O. Mason, E.J. Garboczi and L.R. Pederson, Solid State Ionics 96, 153 (1997).
7. G. Hsieh, S.J. Ford, T.O. Mason and L.R. Pederson, Solid State Ionics 100, 297 (1997).
8. W.J. McCarter, S. Garvin and N. Bouzid, J. Mater. Sci. Lett. 7, 1056 (1988).
9. C.A. Scuderi, T.O. Mason and H.M. Jennings, J. Mater. Sci. 26, 349 (1991).
10. J.T.S. Irvine, D.C. Sinclair and A.R. West, Adv. Mater. 2, 132 (1990).
11. B.A. Boukamp, Equivalent Circuit (EQUIVCRT.PAS) V4.55, University of Twente, Enschede, The Netherlands (1993–96).
12. B.J. Christensen, Microstructure Studies of Hydrating Portland Cement-Based Materials Using Impedance Spectroscopy, Northwestern University, Evanston, Illinois, Thesis, 1993.
13. B.J. Christensen, T.O. Mason and H.M. Jennings, J. Am. Ceram. Soc. 75, 939 (1992).
14. B.J. Christensen, R.T. Coverdale, R.A. Olson, S.J. Ford, E.J. Garboczi, H.M. Jennings and T.O. Mason, J. Am. Ceram. Soc. 77, 2789 (1994).
15. P. Gu, Z. Xu, P. Xie and J.J. Beaudoin, Cem. Concr. Res. 23, 531 (1993).
16. H.A. Miley and U.R. Evans, J. Chem. Soc. 33, 1295 (1937).
17. M.J.N. Pourbaix, Thermodynamics of Dilute Aqueous Solutions, Arnold & Co., London, 1949.
18. J.E.O. Mayne and M.J. Pryor, J. Chem. Soc. 45, 1831 (1949).
19. J. Kruger, Corros. Sci. 29, 149 (1989).
20. H.H. Uhlig and W.R. Revie, Corrosion and Corrosion Control: An Introduction to Corrosion Science and Engineering, p. 79, John Wiley & Sons, New York, 1985.
21. P. Schmuki, M. Büchler, S. Virtanen and H. Böhni, J. Electrochem. Soc. 142, 3336 (1995).
22. S.J. Ford and T.O. Mason, Monitoring the corrosion of reinforcing steel in cement-based systems using impedance spectroscopy. Mechanisms of Chemical Degradation of Cement-Based Materials, K.L. Scrivener and J.F. Young (eds.), p. 125, E & FN Spon, London, 1997.
23. L. Lemoine, F. Wenger and J. Galland, Study of the corrosion of concrete reinforcement by electrochemical impedance measurement. Corrosion Rates of Steel in Concrete, N. S. Berke, V. Chaker and D. Whiting (eds)., p. 118, ASM, Philadelphia, 1990.
24. D.G. John, P.C. Searson and J.L. Dawson, Brit. Corros. J. 16, 102 (1981).
25. G. Reinhard, U. Rammelt and K. Rammelt, Corros. Sci. 26, 109 (1986).
26. L. Hachini, J. Carpio, C. Fiaud, A. Raharinaivo and E. Triki, Cem. Concr. Res. 22, 56 (1992).
27. P. Gu and J.J. Beaudoin, Adv. Cem. Res. 10, 43 (1998).
28. P. Gu, S. Elliott, R. Hristova, J.J. Beaudoin, R. Brousseau, and B. Baldock, ACI Mater. J. 5, 385 (1997).
29. L. Hachani, C. Fiaud, E. Triki and A. Raharinaivo, Brit. Corros. J. 29, 122 (1994).
30. S.J. Ford, Monitoring the Corrosion of Reinforcing Steel in Cement-Based Systems Using Impedance Spectroscopy, Northwestern University, Evanston, Illinois, Thesis, 1998.
31. K.Wiegrink, S. Maritkunte and S.P. Shah, ACI Mater. J. 93, 409 (1996).
32. P.-W. Chen and D.D.L. Chung, Composites B 27, 11 (1996).